JOC The Journal of Organic Chemistry

Article

pubs.acs.org/joc

Elucidating Latent Mechanistic Complexity in Competing Acid-Catalyzed Reactions of Salicylaldehyde-Derived Baylis–Hillman Adducts

Temitope O. Olomola,[†] Rosalyn Klein,[†] Mino R. Caira,[‡] and Perry T. Kaye*[,†]

[†]Department of Chemistry and Centre for Chemico- and Biomedicinal Research, Rhodes University, Grahamstown 6140, South Africa

[‡]Department of Chemistry, University of Cape Town, Rondebosch 7701, South Africa

Supporting Information

ABSTRACT: ^{1}H NMR-based kinetic studies have revealed the latent mechanistic complexity of deceptively simple hydrochloric acid-catalyzed reactions of salicylaldehyde-derived Baylis–Hillman adducts. Reactions conducted at 0 °C afforded 2-(chloromethyl)cinnamic acid derivatives as the major products and the corresponding 3-(chloromethyl)coumarin derivatives as the minor products. In reactions conducted in refluxing acetic acid, however, the 3-(chloromethyl)-coumarin derivatives are the sole products. Variable-temperature ^{1}H NMR analysis permitted the determination of the rate constants and kinetic parameters involved in the pseudo-first-order formation of (*Z*)-2-(chloromethyl)-3-(2-hydroxyphenyl)-2-propenoic acid. The kinetic data clearly preclude the operation of classical kinetic versus thermodynamic control and indicate the operation of three independent reaction pathways. Theoretical studies of these pathways undertaken at the B3LYP/6-31G(d) level permitted rationalization of the experimental data and provided insights into the possible mechanism of the enzymic *E*–*Z* isomerization and cyclization of (*E*)-cinnamic acid analogues to afford coumarins.

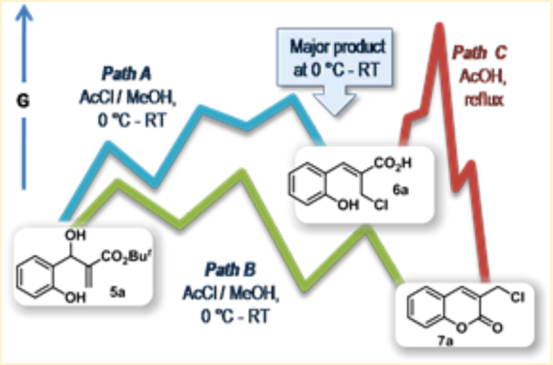

INTRODUCTION

Numerous applications of Baylis–Hillman[1] (or Morita–Baylis–Hillman[2]) methodology continue to be published, and the reaction has been the subject of regular reviews.[3] Our contributions in this area have focused on the synthesis of benzannulated heterocycles, including quinolines,[4] coumarins,[5] and chromenes,[6] and their structural elaboration to compounds with medicinal potential. We have recently reported the synthesis[7] and preliminary evaluation[8] of Baylis–Hillman-derived coumarin–AZT conjugates, such as compound **1**, as potential dual-action HIV-1 protease/reverse transcriptase (PR/RT) inhibitors. Structural similarities between the HIV-1 integrase (IN) and RNase H active sites[9] have prompted research on the development of dual-action RT/IN inhibitors, and Wang et al.[10] reported the synthesis of the HIV-1 RT/IN inhibitor **2**, which exhibited encouraging inhibitory activities (RT, IC_{50} = 57 nM; IN, IC_{50} = 2.4 μM). The apparent HIV-1 IN inhibition activity of L-chicoric acid (**3**) and caffeic acid phenethyl ester has been attributed to the presence of the cinnamate ester moieties,[11] and we have been examining the use of Baylis–Hillman adducts to access cinnamate ester–AZT conjugates, such as compounds **8** (Scheme 1), as potential dual-action HIV-1 RT/IN inhibitors.

We have previously observed[12] that treatment of methyl vinyl ketone (MVK)-derived Baylis–Hillman adducts with HCl

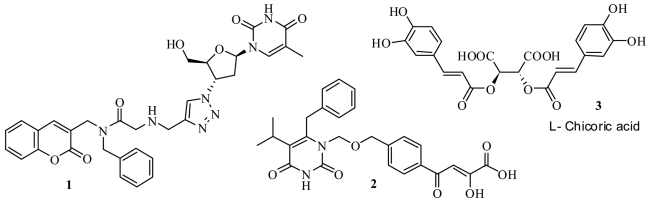

afforded α-chloromethyl-α,β-unsaturated products, apparently via a conjugate addition–elimination pathway, and it seemed reasonable to explore this approach to access the desired cinnamate ester–AZT conjugates **8a–e** (Scheme 1). The concomitant formation of both 2-(chloromethyl)cinnamic acids **6a–e** and 3-(chloromethyl)coumarin derivatives **7a–e** and the ready cyclization of compound **6a** to give coumarin derivative **7a** at elevated temperature prompted us to undertake detailed kinetic and theoretical studies to elucidate the mechanistic details. While some attention has been given to studying the mechanism of the Baylis–Hillman reaction per se,[13] relatively little appears to have been given to transformations of the resulting versatile multifunctional adducts. In this paper, we discuss the results of our experimental kinetic and theoretical

Received: October 15, 2015
Published: December 14, 2015

DOI: 10.1021/acs.joc.5b02372
J. Org. Chem. 2016, 81, 109–120

Scheme 1

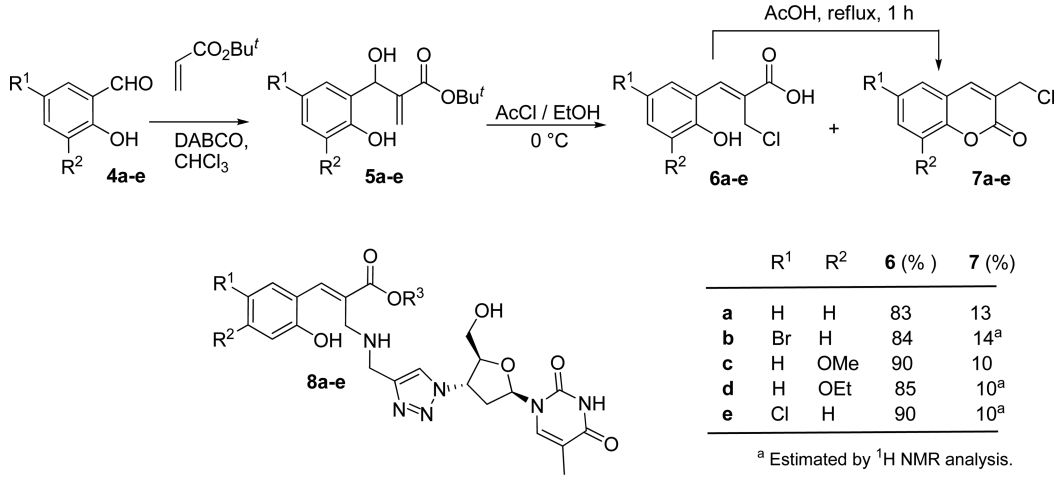

	R1	R2	6 (%)	7 (%)
a	H	H	83	13
b	Br	H	84	14[a]
c	H	OMe	90	10
d	H	OEt	85	10[a]
e	Cl	H	90	10[a]

[a] Estimated by ^{1}H NMR analysis.

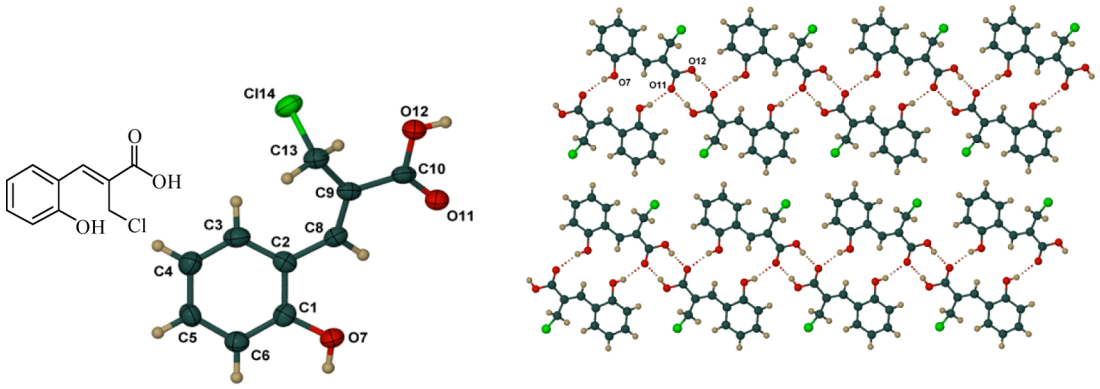

Figure 1. Crystal structure of cinnamic acid derivative **6a**, showing the crystallographic numbering and the crystal packing arrangement. Thermal displacement ellipsoids are drawn at the 50% probability level.

studies of the formation of compounds **6a** and **7a** from the Baylis–Hillman adduct **5a**.

RESULTS AND DISCUSSION

Unlike their methyl and ethyl ester analogues, the *tert*-butyl acrylate-derived Baylis–Hillman adducts **5a–e** are isolable, permitting controlled subsequent elaboration,[14] and they were prepared from the corresponding 2-hydroxybenzaldehydes **4a–e** as described previously.[14] The resulting adducts **5a–e** were treated with HCl [generated in situ by adding acetyl chloride CAUTIOUSLY (!) to dry ethanol at 0 °C; Scheme 1]. In each case, two products were isolated in excellent overall yield (95–100%): a 2-(chloromethyl)cinnamic acid derivative **6** as the major product and the corresponding 3-(chloromethyl)-coumarin **7**. Interestingly, refluxing the crude mixture of compounds **6a** and **7a** in acetic acid for 1 h resulted in complete conversion to the coumarin derivative **7a**. In all cases, the assigned structures are supported by the HRMS, elemental, and NMR spectroscopic data. Compounds **6a** and **7a** were separated by fractional recrystallization, and the structure of compound **6a** was confirmed unequivocally by single-crystal X-ray analysis, which indicated a *Z* configuration about the double bond (Figure 1).

Salient molecular parameters of **6a** include the length of the C8–C9 double bond [1.347(5) Å] and the C3–C2–C8–C9 dihedral angle [29.8(6)°] between the two planar residues. In the crystal, the unique intermolecular hydrogen bonds are O7–H7···O11^{i} (i = 1 − *x*, −*y*, −*z*) and O12–H12···O11^{ii} (ii = −*x*, 1 − *y*, −*z*) with O···O distances of 2.901(4) and 2.579(4) Å, respectively. These create infinite ribbons (portions of two ribbons are shown in Figure 1) that contain alternating centrosymmetric $R_2^2(8)$ H-bonded motifs (the carboxylic acid dimers)[15] and $R_2^2(16)$ motifs.[16] A layered crystal structure results, with only van der Waals forces providing cohesion between successive layers.

After the structures of the major and minor products **6a–e** and **7a–e**, respectively, were ascertained, attention was given to exploring the mechanistic pathways involved in the formation of these products and the reasons for the observed chemoselectivity. The reaction of the parent system **5a** with HCl in methanol-d_4 was monitored by ^{1}H NMR spectroscopy using the signals summarized in Table 1 as probes for the substrate **5a**, the products **6a** and **7a**, and the putative intermediates **10a** and **13a**.

Table 1. Origins and Ranges of ^{1}H NMR Chemical Shifts Used as Probes To Determine the Concentrations of the Substrate, Intermediates, and Products in Methanol-d_4

compound	signal	δ range (ppm)
5a	3′-methylene	5.797–5.866
10a	ArH	7.933–8.029
6a	3′-methylene	4.565–4.513
7a	ArH	8.286–8.357
13a	4-H	5.585–5.667

DOI: 10.1021/acs.joc.5b02372
J. Org. Chem. 2016, 81, 109–120

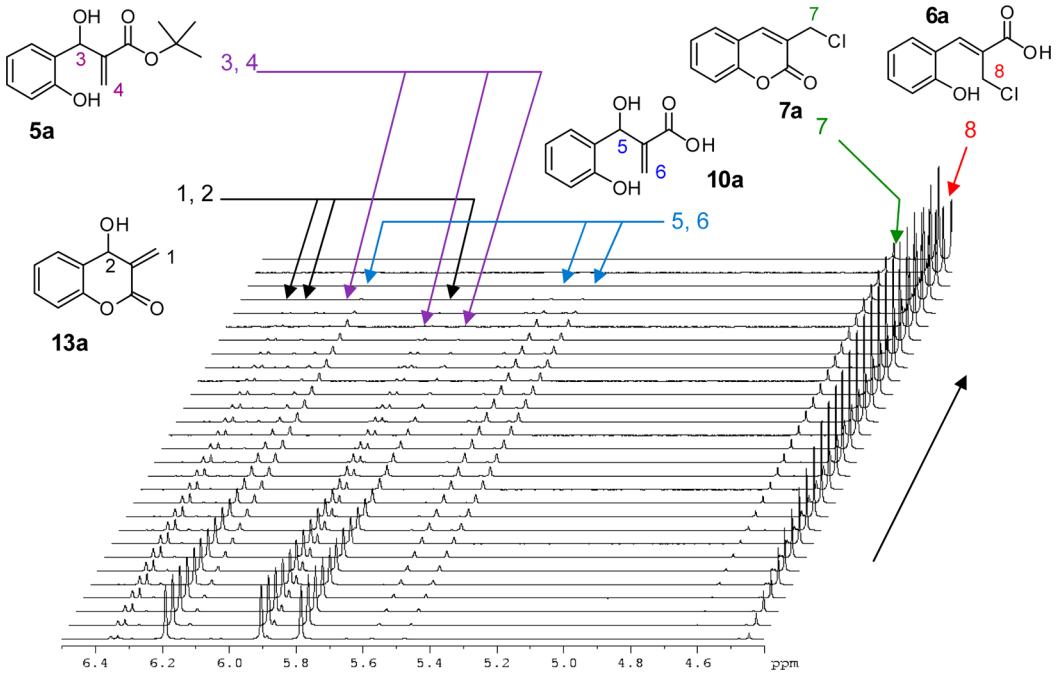

Figure 2. Partial time-dependent 600 MHz ^{1}H NMR spectra selected at 300 s intervals from the commencement of the reaction of the Baylis–Hillman adduct **5a** with in situ-generated HCl in methanol-d_4 at 276.2 K, illustrating some of the signals assigned to structures **5a**, **6a**, **7a**, **10a**, and **13a**.

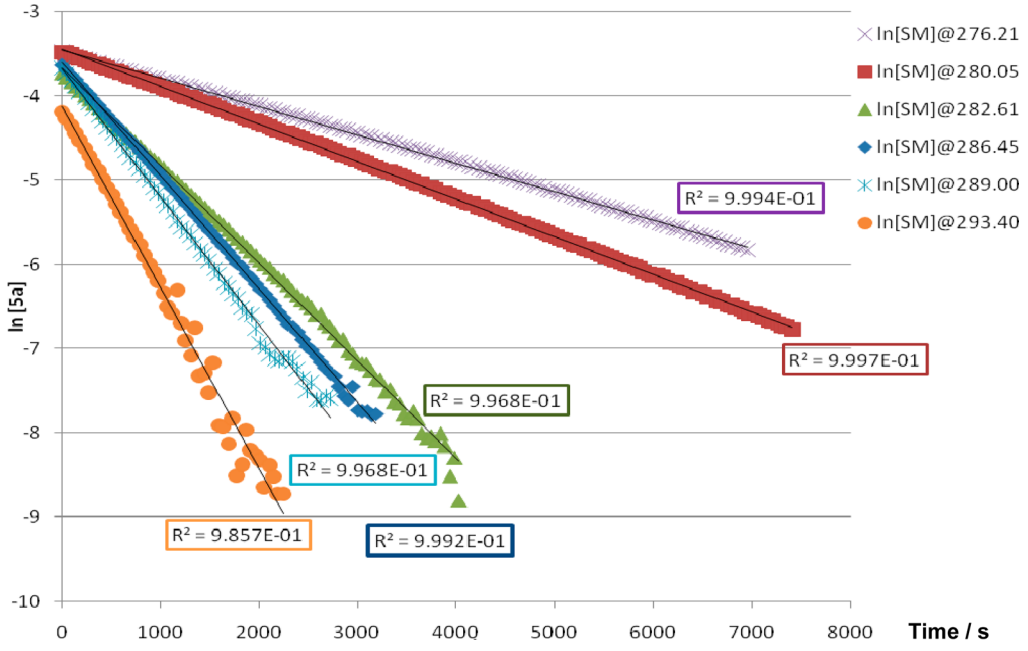

Figure 3. Logarithmic pseudo-first-order kinetic plots reflecting the consumption of the substrate **5a** at different temperatures (276.2–293.4 K); [HCl] = 2.35 M.

A partial stack plot reflecting changes in the concentrations of the substrate **5a** and the major product **6a** is shown in Figure 2. Analysis of the ^{1}H NMR data reveals that consumption of substrate **5a** follows pseudo-first-order kinetics over a range of temperatures (276.2–293.4 K; Figure 3). It is also apparent that the transformation of intermediate **10a** to compound **6a** from 9000 s onward follows pseudo-first-order kinetics (Figure 4). Arrhenius (R^2 = 0.8848; Figure 5) and Eyring (R^2 = 0.8783) plots of the rate constants for the consumption of intermediate **10a** obtained at different temperatures (276.2–293.4 K; Table 2) afforded the kinetic parameters [E_a, $\Delta G^{\ddagger}$ (at 298 K), $\Delta H^{\ddagger}$, and $\Delta S^{\ddagger}$; Table 4]. Similar treatment of the data for the pseudo-first-order consumption of intermediate **13a** (leading to the minor product **7a**) provided the corresponding rate constants at different temperatures (Table 3), and Arrhenius (R^2 = 0.9436; Figure 6) and Eyring (R^2 = 0.9402) plots afforded the kinetic parameters (Table 4).

While the rate constants (k_{obs}) for the consumption of compound **10a** at different temperatures are ca. 6 times smaller than those for compound **13a** (Tables 2 and 3), the corresponding Eyring plots and Arrhenius plots (Figures 5 and 6) exhibit almost identical slopes. As a result, the E_a and $\Delta H^{\ddagger}$

DOI: 10.1021/acs.joc.5b02372
J. Org. Chem. 2016, 81, 109–120

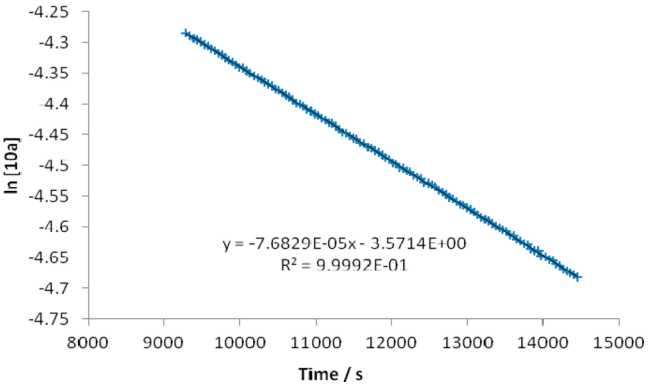

Figure 4. Logarithmic pseudo-first-order kinetic plot from 9000 s onward reflecting the consumption of intermediate **10a** leading to the major product **6a** at 286.45 K; [HCl] = 2.35 M.

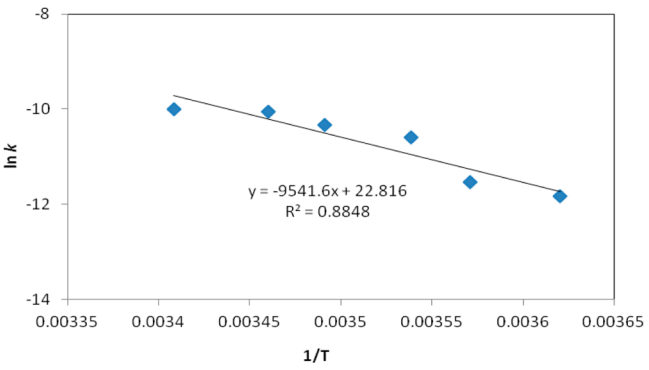

Figure 5. Arrhenius plot (ln k against $1/T$) for the consumption of intermediate **10a** leading to the major product **6a**.

values for the two reactions correspond almost exactly to two decimal places (Table 4)!

In competing reactions, the observation of a temperature-dependent change in the identity of the major product often suggests the operation of classical kinetic versus thermodynamic control. In this case, however, careful examination of the consolidated kinetic data (Figure 7) challenges such an assumption on several grounds, viz., (i) the apparent absence of a *common* intermediate; (ii) the absence of any evidence of reversibility (**5a** ⇄ **6a** ⇄ **7a**) under the reaction conditions; and (iii) the relative rates and sequence of formation of the products **6a** and **7a**. The fact that formation of the minor product **7a** decreases rapidly and then ceases altogether following consumption of the substrate **5a** indicates that it is produced independently of the major product **6a**. In the absence of water (in the early stages of the reaction, at least), cleavage of the ester moiety in protonated ester **9a** is expected to involve *O*-alkyl cleavage to afford carboxylic acid intermediate **10a** (Scheme 2).

On the other hand, cyclization via path B (described below) is proposed to involve *O*-acyl cleavage, i.e., acyl substitution to afford the cyclized intermediate **12a** followed by dehydration to afford coumarin derivative **13a**. While the rate of formation of the major product, 2-(chloromethyl)cinnamic acid **6a**, clearly depends on the concentration of cinnamic acid intermediate **10a**, the rate of formation of the minor product, 3-(chloromethyl)coumarin **7a**, depends on the concentration of cyclic intermediate **13a**, which reaches a maximum *before* intermediate **10a**. Once intermediate **13a** is consumed, further production of the minor product **7a** ceases. We have shown, however, that the transformation **6a** → **7a** can be effected at elevated temperature in refluxing acetic acid. Consequently, on the basis of a combination of a priori considerations and the consolidated ^{1}H NMR kinetic data illustrated in Figure 7, the transformations are considered to involve ester cleavage and conjugate addition−elimination (or an S_N' reaction) (path A; Scheme 2); cyclization−dehydration, i.e., lactonization (path B); and isomerization−cyclization (path C).

In order to elucidate the mechanistic implications of these pathways more fully, theoretical studies at the B3LYP/6-31G(d) level were undertaken using Gaussian 03.[17] In all, over 20 stationary-state structures were located, geometry-optimized, and characterized as substrates, products, or intermediates (with no imaginary frequencies) and transition-state complexes (with a single imaginary frequency). The results of these computational studies are summarized in Table 5 and illustrated graphically in Figures 8−11.

Path A: Formation of the Major Product 6a via *O*-Alkyl Cleavage. A relatively low energy transition-state complex (**TS I**) was located for the initial HCl-catalyzed *O*-alkyl cleavage of the substrate **5a**, consistent with the rapid formation of *β*-hydroxy acid intermediate **10a** (Figure 8). The transition-state complex is stabilized by extended hydrogen bonding between the phenolic and alcohol hydroxyl groups and the carboxylic acid carbonyl oxygen. The chloride anion is not only hydrogen-bonded to the incipient carboxylic acid proton (O−H···Cl = 1.77 Å) but also spatially poised (2.25 Å away) to remove a proton from the essentially trigonal-planar *tert*-butyl cation and thus release isobutylene. Not surprisingly, the transition-state complex **TS I** collapses to a stable arrangement of the three discrete species, viz., intermediate **10a**, isobutylene, and HCl, as depicted in Figure 8. Conjugate addition of HCl to intermediate **10a** leads to intermediate enediol **11a** via transition-state complex **TS II**, in which the reacting moieties are engaged in a delocalized six-center association. The kinetic parameters calculated using the stable three-component "complex" of **10a**, isobutylene, and HCl as the substrate afford a free energy of activation that is very close to the experimentally determined value for the consumption of **10a** and a positive entropy of activation (Table 4), consistent with loss of isobutylene from the "complex".

Table 2. Rate Constant Data (k_{obs}) at Various Temperatures Used for the Consumption of 10a

T (K)	k_{obs} (s^{-1})	R^2	k (M^{-1} s^{-1})[a]	$1/T$ (K^{-1})	ln k	ln(k/T)
276.21	0.000017	0.999162	7.23401×10^{-6}	0.003620434	−11.83671704	−17.45787849
280.05	0.000023	0.999498	9.78719×10^{-6}	0.003570791	−11.53443617	−17.16940433
282.61	0.000059	0.999766	2.51063×10^{-5}	0.003538445	−10.59239294	−16.2364608
286.45	0.000077	0.999916	3.27658×10^{-5}	0.003491011	−10.32612496	−15.98368897
289.00	0.000102	0.999879	4.34041×10^{-5}	0.003460208	−10.04495757	−15.71138426
293.40	0.000107	0.999459	4.55317×10^{-5}	0.003408316	−9.997101552	−15.67863842

[a] $k = k_{obs}/[HCl]$; [HCl] = 2.35 M.

DOI: 10.1021/acs.joc.5b02372
J. Org. Chem. 2016, 81, 109−120

Table 3. Rate Constant Data (k_{obs}) at Various Temperatures Used for the Consumption of 13a

T (K)	k_{obs} (s^{-1})	R^2	k (M^{-1} s^{-1})[a]	$1/T$ (K^{-1})	ln k	ln(k/T)
276.21	0.000099	0.999382	4.21275E-05	0.003620434	−10.07481054	−15.69597198
280.05	0.000122	0.999674	5.19147E-05	0.003570791	−9.865909341	−15.5008775
282.61	0.000254	0.993677	0.000108085	0.003538445	−9.132596119	−14.77666397
286.45	0.000394	0.997412	0.000167659	0.003491011	−8.693579477	−14.35114348
289.00	0.000504	0.997882	0.000214467	0.003460208	−8.447354118	−14.11378081
293.40	0.000621	0.993978	0.000264254	0.003408316	−8.238599304	−13.92013617

[a] $k = k_{obs}/[HCl]$; [HCl] = 2.35 M.

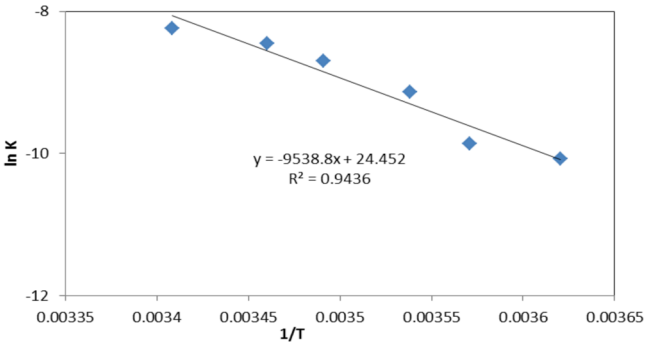

Figure 6. Arrhenius plot (ln k against $1/T$) for the consumption of intermediate **13a** leading to the minor product **7a**.

Dehydration of enediol **11a** via transition-state complex **TS III** finally affords the major product **6a**. Transition-state complex **TS III**, which corresponds to the highest point of the free energy profile, is stabilized by an interesting hydrogen-bonding network—a level of molecular organization that would account for the *experimentally observed* negative entropy of activation for the *overall* transformation **10a** → **6a** (Table 4). We thus conclude that rapid and irreversible *O*-alkyl cleavage of the substrate **5a** affords the stable *β*-hydroxy acid intermediate **10a**, which is slowly consumed in the reaction sequence **10a** → **11a** → **6a**, a pattern consistent with the experimental results illustrated in Figure 7. [The preference for a conjugate addition−elimination sequence rather than S_N' displacement of the protonated hydroxyl group by the chloride anion is supported by comparative studies on related systems[12] and the relative condensed local softness values for the carbonyl (3.97) and hydroxylic (0.91) carbons using the electrophilic Fukui functions (f^+)[18] evaluated at a B3LYP/6-31G(d) level.] Noteworthy in the formation of the major isomer **6a** is the multifaceted role of HCl in (i) acid catalysis of *O*-alkyl cleavage of *tert*-butyl ester **5a**, (ii) deprotonation (by the conjugate base Cl^-) of the *tert*-butyl cation, (iii) conjugate addition to *α*,*β*-unsaturated acid **10a**, and (iv) acid catalysis of the dehydration of enediol **11a**.

Path B: Formation of the Minor Product 7a via *O*-Acyl Cleavage. Reversible HCl-catalyzed cyclization of Baylis−Hillman adduct **5a** to tetrahedral intermediate **12a** involves nucleophilic attack of the phenolic oxygen on the ester acyl center via transition-state complex **TS IV** (Figure 9). In this process, HCl catalyzes the transformation by simultaneously (i) protonating the ester carbonyl oxygen, thus enhancing the electrophilicity of the acyl carbon; (ii) deprotonating the phenolic group, thus enhancing the nucleophilicity of the phenolic oxygen; and (iii) facilitating formation of a six-center hydrogen-bonded chelate in which the reactive centers are ideally disposed relative to each other at a distance of 1.78 Å, thus decreasing the entropic demand. The next step, which proceeds via transition-state complex **TS V**, involves acid-catalyzed loss of *tert*-butyl alcohol from intermediate **12a** and formation of 4-hydroxy-3-methylenepyran-2-one **13a**. The structural changes associated with the imaginary frequency (363.2i cm^{-1}) for transition-state complex **TS VI** in the final step (**13a** → **7a**) exemplify a classic acid-catalyzed S_N2' reaction involving (i) protonation of the 3-hydroxyl oxygen, (ii) nucleophilic attack by Cl^- at the terminal vinylic center, (iii) migration of the double bond, and (iv) loss of the *syn* leaving group as neutral H_2O. The minor product, 3-chloromethylcoumarin **7a**, is thus obtained in what is clearly an overall exergonic process ($\Delta G^\circ = -28.18$ kcal mol^{-1}). The calculated and experimental free energies of activation for the consumption of intermediate **13a** correlate closely (Table 4); the $\Delta S^\ddagger$ values are both negative, but the theoretical model underestimates the E_a and $\Delta H^\ddagger$ values.

Comparative free energy profiles for paths A and B are presented on the same scale in Figure 10. It is immediately apparent that the theoretical data seem to indicate that the major product **6a** is *neither* thermodynamically *nor* kinetically favored! In fact, the major product **6a** is calculated to be significantly less stable (by $\Delta G^\circ = 42.8$ kcal mol^{-1}) than the minor product **7a**, and the transition-state complexes leading to the major product (**6a**; path A) have consistently higher free energies than those leading to the minor product (**7a**; path B). However, the apparent anomalies presented by this comparison of the theoretical results with the experimental data can be explained.

First, it may be argued that following the rapid formation of intermediate carboxylic acid **10a** and the concomitant irreversible loss of isobutylene in the first step in path A, consumption of

Table 4. Kinetic Parameters Obtained from Arrhenius and Eyring Plots of the Data for Consumption of Intermediates 10a and 13a

	consumption of **10a**		consumption of **13a**	
	experimental[a]	theoretical[b,c]	experimental[a]	theoretical[b]
$\Delta G^\ddagger$ (kcal mol^{-1})	22.89 ± 0.31[b]	23.65	21.91 ± 0.20[b]	21.04
$\Delta S^\ddagger$ (cal mol^{-1} K^{-1})	−15.09 ± 6.1	20.83	−11.84 ± 4.10	−35.75
E_a (kcal mol^{-1})	18.96 ± 0.30	29.27	18.95 ± 0.20	10.97
$\Delta H^\ddagger$ (kcal mol^{-1})	18.39 ± 0.30	29.86	18.39 ± 0.20	10.38

[a] Errors were calculated from the respective standard errors for the slope and intercept for each graph. [b] At 298.15 K. [c] Results are based on the use of the stable three-component complex of **10a**, isobutylene, and HCl.

DOI: 10.1021/acs.joc.5b02372
J. Org. Chem. 2016, 81, 109−120

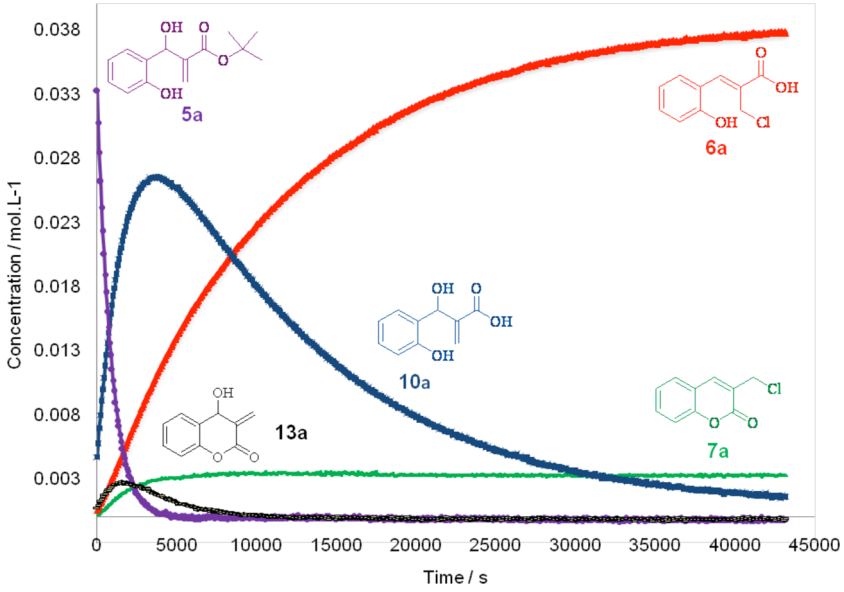

Figure 7. Plots of concentrations against time (from 600 MHz ^{1}H NMR spectra in methanol-d_4) for the reaction of the Baylis–Hillman adduct **5a** with in situ-generated HCl at 276.2 K, showing the consumption of the substrate and the formation of intermediates **10a** and **13a**, the major product **6a**, and the minor product **7a**.

Scheme 2. Proposed Reaction Pathways for the Formation of Compounds 6a and 7a from the Baylis–Hillman Adduct 5a in HCl/EtOH and the Formation of 7a from 6a in Refluxing AcOH

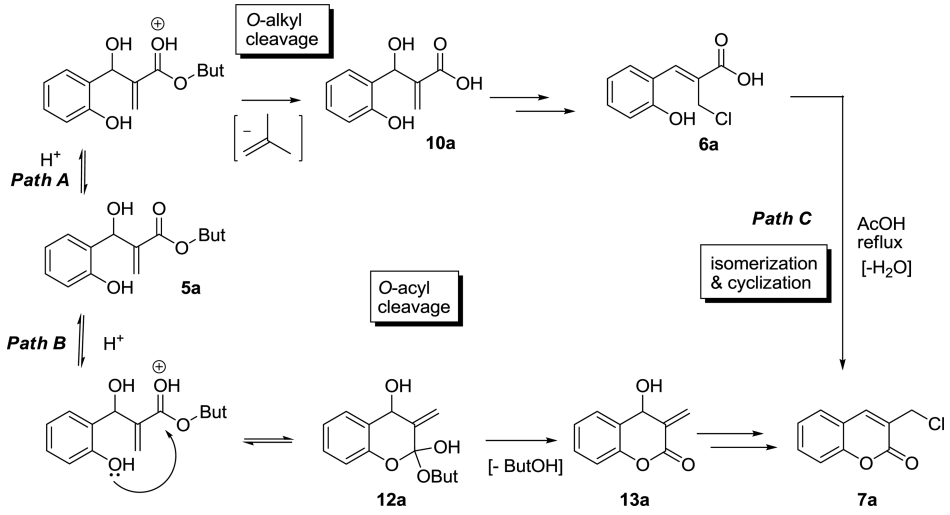

intermediate **10a** leads slowly to the product **6a**; the rate of *irreversible* consumption of the substrate **5a** in this reaction path may be expressed by eq 1. Second, the rate-determining step in path B (i.e., the second step via transition-state complex **TS V**) is preceded by what is expected to be an equilibrium between the substrate **5a** and the cyclized tetrahedral intermediate **12a**; the rate of this reaction is therefore proportional to the product of the equilibrium constant K_{B1} and the rate constant k_{B2} (eq 2). Under the assumption of pseudo-first-order reactions (loss of HCl is considered to be minimal), the free energy of activation for the first step in path A ($\Delta G^{\ddagger}$ = 24.55 kcal mol^{-1}) corresponds to a rate constant $k_{A1} = 6.32 \times 10^{-6}$ s^{-1}. In path B, the free energy difference between **5a** and **12a** (ΔG° = 7.87 kcal mol^{-1} at 298.15 K) corresponds to an equilibrium constant $K_{B1} = 1.69 \times 10^{-6}$, while the free energy of activation for the *second* step in path B ($\Delta G^{\ddagger}$ = 18.17 kcal mol^{-1}) corresponds to a rate constant $k_{B2} = 3.00 \times 10^{-1}$ s^{-1}; thus, $K_{B1} \times k_{B2} = 5.08 \times 10^{-7}$ s^{-1}. Consequently, the substrate **5a** should be consumed more rapidly (ca. 12-fold) in the irreversible formation of intermediate **10a** in path A than in the formation of intermediate **13a** in the rate-determining second step in path B—a result that corresponds reasonably closely to the *experimentally* determined ratio of the two products (**7a**:**6a** = 1.0:0.11) *at the end of the kinetic run* at 293 K (at which stage, a small concentration of **10a** still remains!). Thus, formation of the minor product **7a** ceases early in the reaction, while formation of the major product **6a** continues slowly until intermediate **10a** is consumed.

path A (**5a** + HCl → **10a**):

$$\text{reaction rate} = k_{A1}[\mathbf{5a}][\text{HCl}] \quad (1)$$

path B (**5a** + HCl → **13a**):

$$\text{reaction rate} = K_{B1} \times k_{B2}[\mathbf{5a}][\text{HCl}] \quad (2)$$

DOI: 10.1021/acs.joc.5b02372
J. Org. Chem. 2016, 81, 109–120

Table 5. B3LYP/6-31G(d) Stationary-State Free Energies and Transition-State Vibrational Frequencies for the Geometry-Optimized Structures Used, *after Mass Balancing*, in Figures 8−11

structure	free energy (G) hartrees	free energy (G) kcal mol^{-1}	frequency (cm^{-1})
	Path A (Figure 8)		
5a	−844.942701	−530209.5718	–
TS I	−1305.710485	−819345.7336	−148.59
10a + HCl + isobutylene	−1305.730337	−819358.1909	–
TS II	−1148.575447	−720742.0045	−148.10
11a	−1148.58451	−720747.6916	–
TS III	−1148.569654	−720738.3693	−902.51
6a	−1072.203627	−672817.9619	–
isobutylene	−157.117209	−98592.54126	–
H_2O	−76.405453	−47945.14761	–
HCl	−460.806901	−289160.708	
	Path B (Figure 9)		
5a	−844.942701	−530209.5718	–
TS IV	−1305.713788	−819347.8063	−388.58
12a	−1305.737054	−819362.4059	–
TS V	−1305.708105	−819344.2401	−174.60
13a	−611.400499	−383659.6214	–
TS VI	−1072.173867	−672799.2872	−363.18
7a	−995.82541	−624889.9051	–
t-BuOH	−233.563639	−146563.4023	–
HCl	−460.806901	−289160.708	
	Path C (Figure 11)		
6a-AcOH	−1301.249682	−816546.5373	–
TS VII	−1301.223523	−816530.1223	−739.44
14a	−1301.221498	−816528.8516	–
TS VIII	−1301.195513	−816512.5458	−111.23
15a	−1301.244558	−816543.322	–
TS IX	−1301.237301	−816538.7681	−716.67
7a	−995.82541	−624889.9051	–
AcOH	−229.047031	−143729.1879	–

Path C: *Z*−*E* Isomerization of 2-(Chloromethyl)-cinnamic Acid Derivative 6a and Subsequent Cyclization To Give 3-(Chloromethyl)coumarin 7a. Transformation of (*Z*)-2-(chloromethyl)cinnamic acid derivative **6a** to 3-(chloromethyl)coumarin **7a** requires a change in the double-bond geometry from *Z* to *E* prior to cyclization. Although it does not occur at low temperature (Figure 7), the transformation **6a** → **7a** is readily effected in refluxing acetic acid (bp 117 °C). It is not unreasonable to assume that under these conditions substrate−solvent interactions facilitate both the isomerization and lactonization steps, and the initial stationary-state structure **6a**-AcOH (Figure 11) reflects chelation of an acetic acid molecule with **6a**; an intramoleclar hydrogen-bonding interaction is also evident between chlorine and the cinnamic acid proton. For practical purposes, the hydrogen-bonded chelate **6a**-AcOH was treated as the substrate in this reaction. The acetic acid plays a pivotal role as an amphoteric catalyst in the formation of *metastable* quinone methide intermediate **14a**, via transition-state complex **TS VII**, simultaneously protonating the cinnamic acid carbonyl oxygen and deprotonating the phenolic group. [The free energy of the metastable species **14a**, which has no imaginary frequencies, is slightly *higher* (by ca. 1 kcal mol^{-1}) than that of the preceding transition-state complex **TS VII**, but its electronic energy is slightly *lower* (also by ca. 1 kcal mol^{-1}).] The π-electron delocalization leading to the quinone methide system **14a** affords a rotatable σ bond that permits $Z \rightarrow E$ isomerization via transition-state complex **TS VIII**, which is characterized by a torsion angle of ca. 90° between the rotating planes. The intermediate structure **15a** was located, in which chelation of the resulting (*E*)-cinnamic acid derivative involves both the hydroxylic and carbonyl oxygens of the acetic acid; intramolecular hydrogen-bonding between chlorine and the cinnamic acid proton is also retained. The reorientation of the chelating moiety in structure **15a** provides a level of preorganization that facilitates cyclization and serves to stabilize the subsequent transition-state complex **TS IX** via an interesting hydrogen-bonding network. In fact, the transition-state complex **TS IX** is characterized by the involvement of no less than eight centers, with acetic acid once more serving as an amphoteric catalyst enhancing *both* the electrophilicity of the acyl carbon by protonating the acyl oxygen *and* the nucleophilicity of the phenolic oxygen by removing the phenolic proton (Figure 12a).

E−*Z* isomerization of cinnamic acid analogues is involved in various established syntheses of coumarin derivatives, including the Perkin,[19] Knoevenagel,[20] and Wittig[21] reactions, and Jeon et al.[22] recently reported the preparation of 3,4-dihydrocoumarins via the *p*-toluenesulfonic acid-catalyzed thermal isomerization and cyclization of cinnamic acid derivatives in sealed tubes at 140 °C. *E*−*Z* isomerization is also involved in the biosynthesis of coumarin analogues from *o*-coumaric acid.[23] In early studies, Haskins et al.[24] reported that the *E*−*Z* isomerization of β-D-glucosyl *o*-hydroxycinnamic acid in sweetclover (*Melilotus alba*) leaves was photochemically, not enzymically, induced. In a more recent study, however, Bayoumi et al.[25] provided a review of

DOI: 10.1021/acs.joc.5b02372
J. Org. Chem. 2016, 81, 109−120

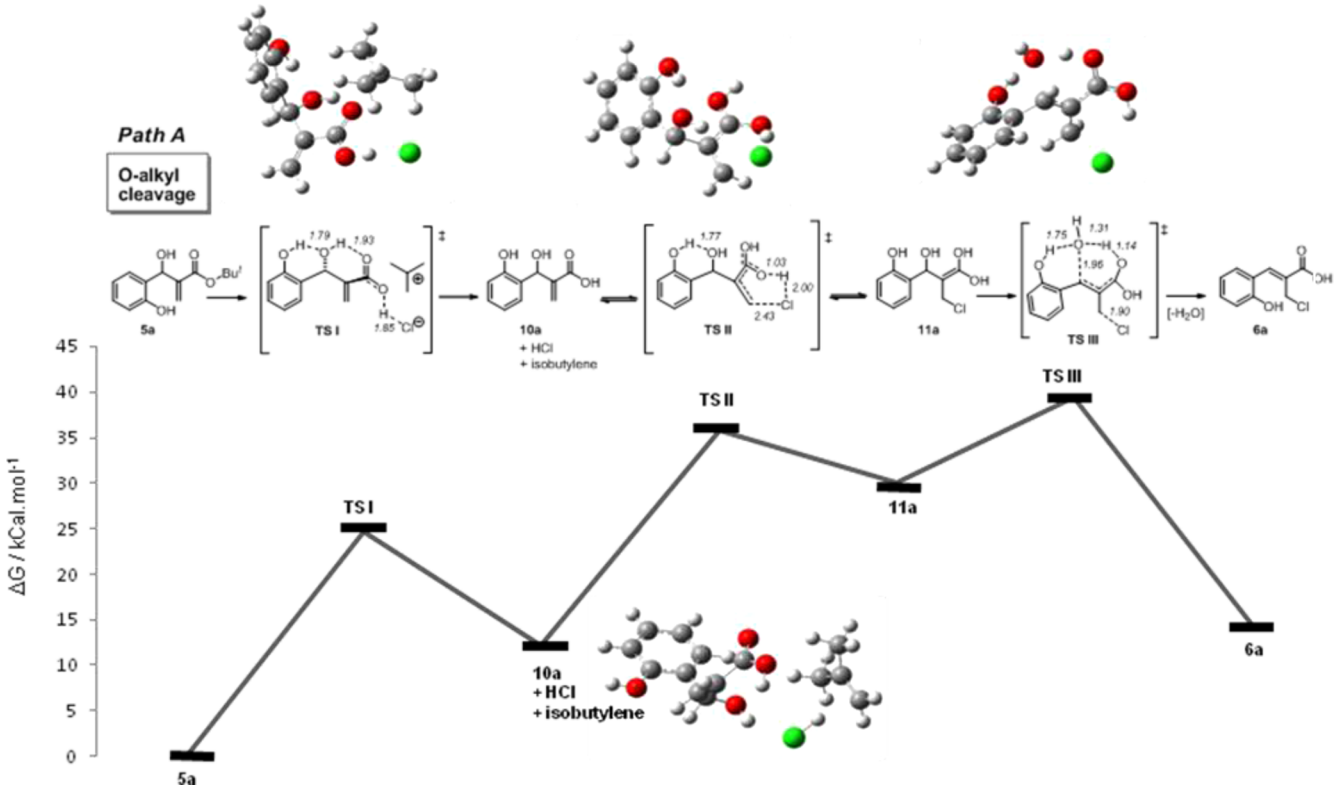

Figure 8. Mass-balanced free energy profile for the formation of the major product **6a** via *O*-alkyl cleavage (path A), showing ball-and-stick structures for the transition states **TS I**–**TS III** and the stable arrangement of the three discrete species **10a**, isobutylene, and HCl, colored according to atom type (H, white; C, gray; O, red; Cl, green).

differing opinions concerning enzymic or photochemical involvement in the *E*–*Z* isomerization stage of the biosynthesis of coumarin analogues and clearly demonstrated that *E*–*Z* isomerization of isotopically substituted (*E*)-cinnamic acid in cassava (*Manihot esculenta* Crantz) roots is enzymatically, not photochemically, induced! Such isomerizations are attributed to addition–σ-rotation–elimination sequences. Somewhat surprisingly, no attention appears to have been given to the possibility of an enzymatically generated quinone methide intermediate (e.g., structure **16** in Figure 12b) in which appropriately placed amino acid residues or water molecules in an enzyme active site could provide the hydrogen-bonding environments needed to mediate *both* *E*–*Z* isomerization *and* subsequent cyclization via the proximate *o*-phenolic oxygen and the acyl center (as in structure **17**)—clearly entropically advantageous arrangements.

CONCLUSIONS

^{1}H NMR-based kinetic studies of the hydrochloric acid-catalyzed reaction of the salicylaldehyde-derived Baylis–Hillman adduct **5a** have permitted evaluation of the kinetic parameters for the pseudo-first-order dissociation of intermediates **10a** and **13a** leading to the major and minor products **6a** and **7a**, respectively. Independent pathways have been identified for the formation of these products at low temperatures (276.2–293.4 K), and detailed theoretical studies have provided important insights into the mechanistic implications and permitted rationalization of their latent complexity. Theoretical studies of the acetic acid-catalyzed thermal cyclization of **6a** to give **7a** have indicated the possible involvement of a hydrogen-bonded quinone methide transition-state complex in the critical cyclization step—an observation of potential significance in the biosynthesis of coumarin analogues from *o*-coumaric acid.

EXPERIMENTAL SECTION

General Information. NMR spectra were recorded at 303 K (except where described otherwise for kinetics experiments) in DMSO-d_6, $CDCl_3$, or methanol-d_4 and calibrated using solvent signals [δ_H: 7.26 ppm for residual $CHCl_3$, 2.50 ppm for residual DMSO, and 3.31 ppm for residual methanol; δ_C: 77.0 ppm for $CDCl_3$ and 39.5 for DMSO-d_6]; coupling constants are given in hertz. Melting points were measured using a hot-stage apparatus and are uncorrected. IR spectra were recorded with a diamond window, and compounds were analyzed neat.

The known *tert*-butyl 3-hydroxy-3-(2-hydroxyphenyl)-2-methylenepropanoate esters **5a**–**e**[14] were prepared using both established and microwave-assisted methods; the latter afforded the products much more rapidly (in 1 h) but seldom in better yield than the conventional approach (4–21 days). The coumarins **7a**–**e** are also known.[5]

Hydrochloric Acid-Catalyzed Reactions of the Baylis–Hillman Adducts 5a–e. The general procedure is illustrated by the following example.

Acetyl chloride (1.2 mL) was added dropwise to dry methanol (1.0 mL) cooled in an ice bath (CAUTION! exothermic reaction). The mixture was left to stir for 30 min, and *tert*-butyl 3-hydroxy-3-(2-hydroxyphenyl)-2-methylenepropanoate (**5a**) (0.50 g, 2.0 mmol) dissolved in dry methanol (2 mL) was then added. The mixture was left to stir overnight. Water (20 mL) was added to the crude mixture, which was then extracted with $CHCl_3$ (2 × 20 mL) and concentrated in vacuo. Fractional recrystallization from chloroform afforded two products, the major product *(Z)-2-(chloromethyl)-3-(2-hydroxyphenyl)-2-propenoic acid* (**6a**) [pink solid (0.35 g, 83%), mp 129–131 °C (Found: C, 56.22; H, 4.40%. $C_{10}H_9ClO_3$ requires C, 56.49; H, 4.27%); ν_{max}/cm^{-1} 3453 (OH), 1666 (C=O); δ_H (400 MHz, DMSO-d_6) 4.47 (2H, s), 6.90–6.96 (2H, m), 7.28 (1H, t, J = 7.7 Hz), 7.49 (1H, m), 7.96 (1H, s), 10.22 (1H, br s); δ_C (100 MHz, DMSO-d_6) 41.1, 116.7, 120.1,

DOI: 10.1021/acs.joc.5b02372
J. Org. Chem. 2016, 81, 109–120

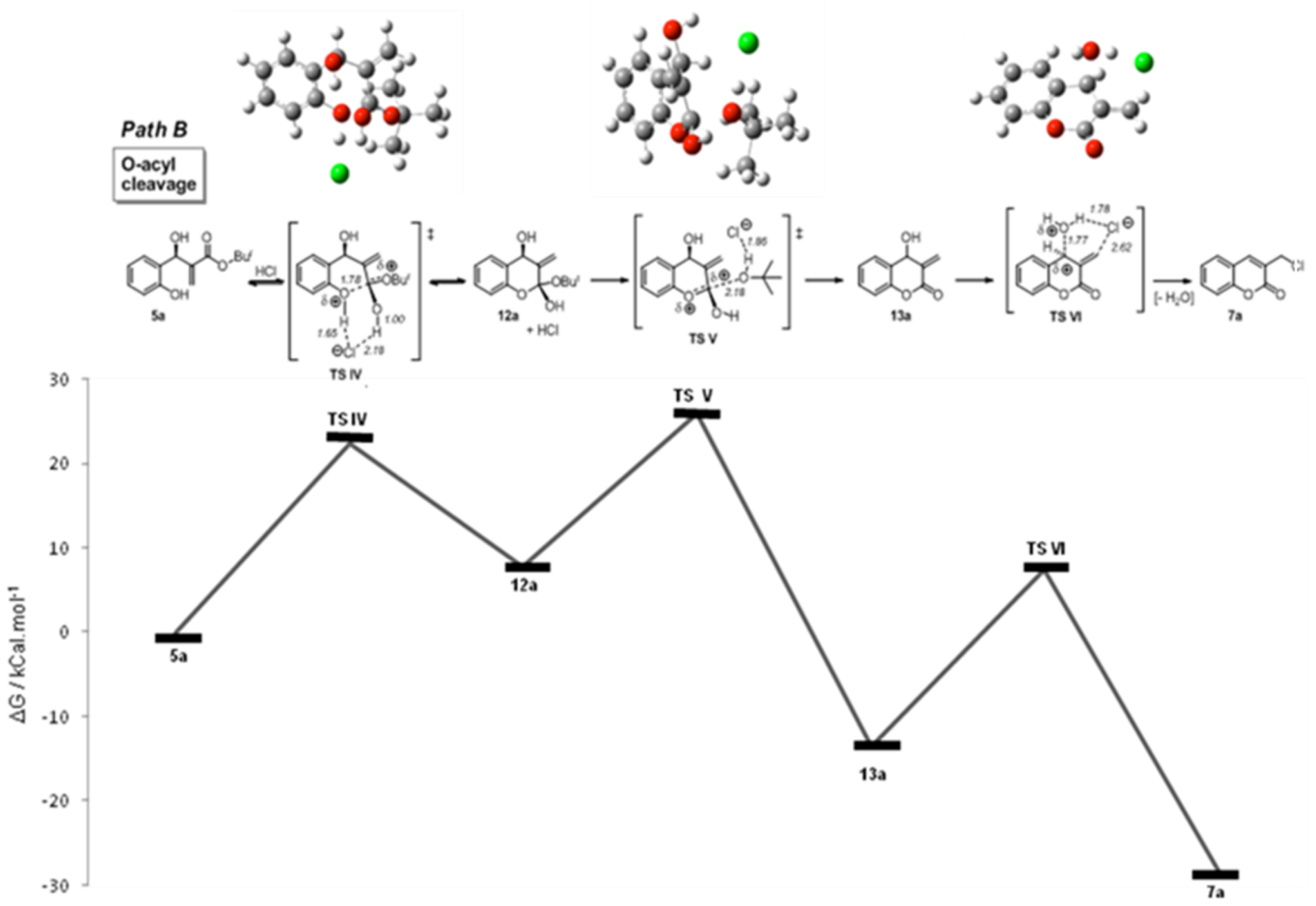

Figure 9. Mass-balanced free energy profile for the formation of the minor product **7a** via *O*-acyl cleavage (path B), showing ball-and-stick structures for the transition states **TS IV**–**TS VI**, colored according to atom type (H, white; C, gray; O, red; Cl, green).

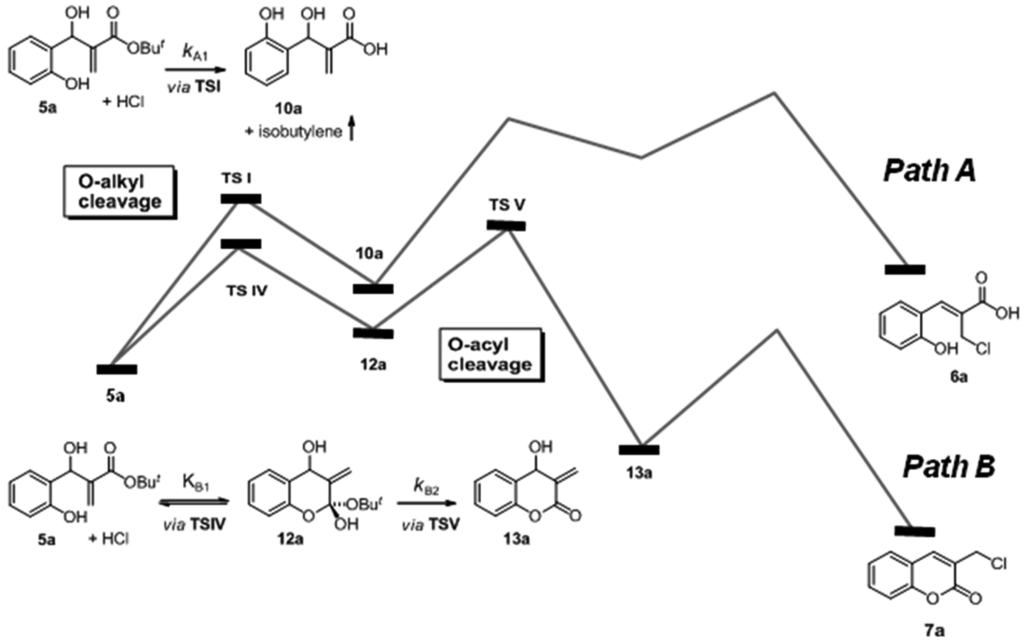

Figure 10. Superimposed mass-balanced free energy profiles for the formation of the major product **6a** via *O*-alkyl cleavage (path A) and the minor product **7a** via *O*-acyl cleavage (path B).

121.8, 128.2, 130.0, 132.3, 139.5, 157.4, 168.2] and the minor product *3-(chloromethyl)coumarin* (**7a**) [pale-yellow solid (0.05 g, 13%)].

Yields and analytical data for the remaining products are as follows:

(Z)-3-(5-Bromo-2-hydroxyphenyl)-2-(chloromethyl)-2-propenoic acid (**6b**) [pale-yellow solid (0.37 g, 84%), mp 146–148 °C (Found: C, 41.29; H, 2.88%. $C_{10}H_8BrClO_3$ requires C, 41.20; H, 2.77%); ν_{max}/cm^{-1}

DOI: 10.1021/acs.joc.5b02372
J. Org. Chem. 2016, 81, 109–120

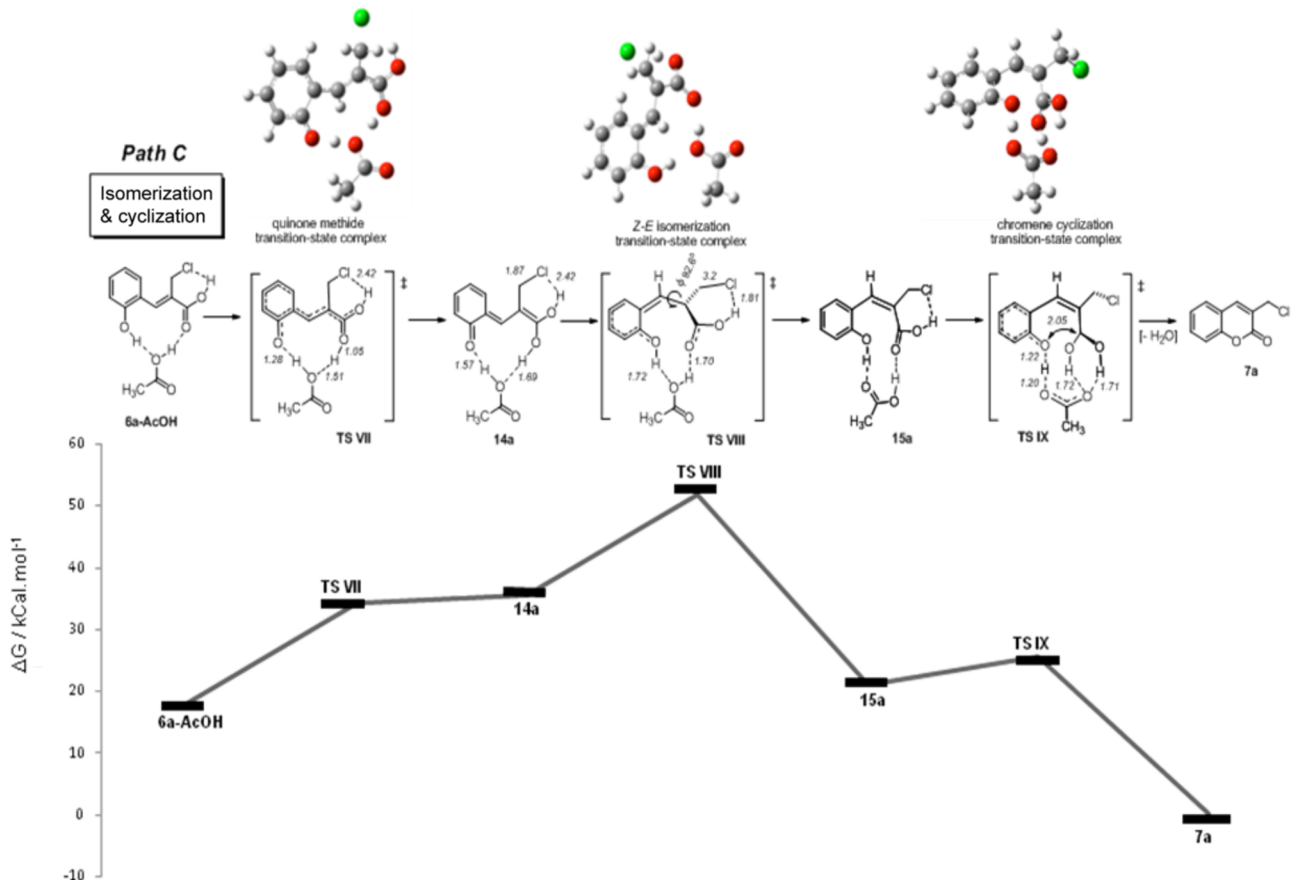

Figure 11. Mass-balanced free energy profile for the *Z*−*E* isomerization of 2-(chloromethyl)cinnamic acid derivative **6a** and subsequent cyclization to give 3-(chloromethyl)coumarin **7a** (path C), showing ball-and-stick structures for the transition states **TS IV**−**TS VI**, colored according to atom type (H, white; C, gray; O, red; Cl, green).

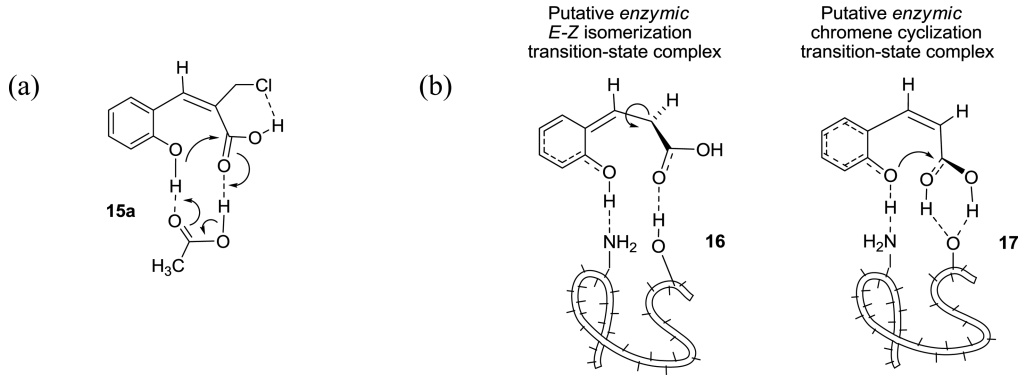

Figure 12. (a) Mechanistic depiction of the role of acetic acid as an amphoteric catalyst in the cyclization of (*Z*)-3-(chloromethyl)-2-(hydroxyphenyl)-2-propenoic acid (**15a**). (b) Putative structures involved in a suggested enzyme-catalyzed *E*−*Z* isomerization of *o*-coumaric acid **16** and the subsequent lactonization of the *Z* isomer **17** to form coumarin.

3421 (OH), 1669 (C═O); δ_H (400 MHz, methanol-d_4) 4.43 (2H, s), 6.81 (1H, d, J = 8.7 Hz), 7.36 (1H, d, J = 8.7 Hz), 7.71 (1H, s), 7.97 (1H, s); δ_C (100 MHz, DMSO-d_6) 40.7, 111.0, 118.7, 124.0, 129.5, 132.1, 134.6, 138.0, 156.6, 167.8] and *6-bromo-3-(chloromethyl)coumarin* (**7b**) (14% estimated by ^{1}H NMR analysis).

(Z)-2-(Chloromethyl)-3-(2-hydroxy-3-methoxyphenyl)-2-propenoic acid (**6c**) [lilac solid (0.39 g, 90%), mp 137−139 °C (Found: C, 54.63; H, 4.80%. $C_{11}H_{11}ClO_4$ requires C, 54.45; H, 4.57%); ν_{max}/cm^{-1} 3499 (OH), 1671 (C═O); δ_H (400 MHz, methanol-d_4) 3.88 (3H, s), 4.47 (2H, s), 6.88 (1H, t, J = 7.9 Hz), 7.00 (1H, d, J = 7.9 Hz), 7.20 (1H, d, J = 7.9 Hz), 8.10 (1H, s); δ_C (100 MHz, methanol-d_4) 40.6, 56.5, 113.8, 120.3, 122.2, 122.6, 129.2, 140.5, 147.2, 149.1, 169.7] and *3-(chloromethyl)-8-methoxycoumarin* (**7c**) [brown solid (0.04 g, 10%)].

(Z)-2-(Chloromethyl)-3-(3-ethoxy-2-hydroxyphenyl)-2-propenoic acid (**6d**) [purple solid (0.37 g, 85%), mp 128−130 °C (Found: C, 56.27; H, 5.10%. $C_{12}H_{13}ClO_4$ requires C, 56.15; H, 5.10%); ν_{max}/cm^{-1} 3489 (OH), 1674 (C═O); δ_H (400 MHz, $CDCl_3$) 1.47 (3H, t, J = 6.9 Hz), 4.15 (2H, q, J = 6.9 Hz), 4.50 (2H, s), 6.07 (1H, br s), 6.92 (2H, m), 7.28 (1H, m), 8.25 (1H, s); δ_C (100 MHz, $CDCl_3$) 14.8, 39.3, 64.8, 113.1, 119.9, 120.4, 121.4, 127.3, 140.7, 145.1, 145.8, 171.3] and *3-(chloromethyl)-8-ethoxycoumarin* (**7d**) (10% estimated by ^{1}H NMR analysis).

DOI: 10.1021/acs.joc.5b02372
J. Org. Chem. 2016, 81, 109−120

(Z)-3-(5-Chloro-2-hydroxyphenyl)-2-(chloromethyl)-2-propenoic acid (**6e**) [pale-yellow solid (0.39 g, 89%), mp 126−128 °C (Found: C, 48.48; H, 3.48%. $C_{10}H_8Cl_2O_3$ requires C, 48.61; H, 3.26%); ν_{max}/cm^{-1} 3408 (OH), 1666 (C═O); δ_H (400 MHz, $CDCl_3$) 4.42 (2H, s), 6.80 (1H, d, J = 8.7 Hz), 7.21 (1H, d, J = 8.7 Hz), 7.55 (1H, s), 8.00 (1H, s); δ_C (100 MHz, methanol-d_4) 40.1, 117.9, 124.3, 125.2, 130.0, 130.3, 131.9, 139.3, 156.5, 169.3 (C═O)] and *6-chloro-3-(chloromethyl)-coumarin* (**7e**) (10% estimated by ^{1}H NMR analysis).

X-ray Analysis of 2-(Chloromethyl)cinnamic Acid Derivative 6a. Crystal data for **6a**: $C_{10}H_9ClO_3$, M = 212.62, 0.25 mm × 0.13 mm × 0.09 mm, triclinic, space group $P\bar{1}$ (No. 2), a = 5.1208(4) Å, b = 7.8498(8) Å, c = 11.9863(12) Å, α = 99.256(4)°, β = 91.114(7)°, γ = 100.217(7)°, V = 467.43(8) Å^3, Z = 2, D_c = 1.511 g cm^{-3}, F_{000} = 220, Mo Kα radiation, λ = 0.71073 Å, T = 173(2) K, $2\theta_{max}$ = 54.9°, 25 716 reflections collected, 2115 unique (R_{int} = 0.0427). Final GOF = 1.044, R_1 = 0.0765, wR_2 = 0.2063, R indices based on 1552 reflections with $I > 2\sigma(I)$, (refinement on F^2), 129 parameters, 0 restraints. Lorentz polarization and absorption corrections applied, μ = 0.383 mm^{-1}, CCDC 1016110.

Kinetic Studies. Kinetic experiments were conducted on a Bruker Biospin 600 MHz NMR spectrometer. Temperature calibration of the spectrometer was carried out between 273 and 333 K, and the temperatures reported for each kinetic run are the corrected values. For each kinetic run, acetyl chloride (0.1 mL) was added to cooled CD_3OD (0.4 mL) in a graduated NMR tube, which was then sealed with a septum, and an initial ^{1}H NMR spectrum was obtained. A solution of compound **5a** (20 mg, 80 μmol) in CD_3OD (0.1 mL) was then added, the total volume of reaction mixture noted, and the tube replaced in the NMR probe. ^{1}H NMR spectra were recorded automatically with a delay of 40 s between acquisitions. Experiments were repeated at six different temperatures between 273 and 295 K.

Computational Studies. All of the density functional theory calculations were performed with the B3LYP hybrid density functional with the 6.31G(d) basis set using the Gaussian 03 program[17] running on an Intel/Linux cluster; Gaussview 4.1[26] and Molden[27] were used for visualization. Stationary-state structures were characterized by vibrational analysis. Substrates, products, and intermediates were characterized by the absence of imaginary frequencies and transition-state complexes by the presence of a single imaginary frequency. Each transition-state structure was confirmed by inspection of the vibration corresponding to the imaginary frequency, calculation of the corresponding IRC path, or in some cases energy minimization of structures close to the transition state. Table 5 summarizes the calculated free energies and, where appropriate, vibrational frequencies for the stationary states involved in paths A, B, and C.

■ ASSOCIATED CONTENT

Supporting Information

The Supporting Information is available free of charge on the ACS Publications website at DOI: 10.1021/acs.joc.5b02372.

Copies of ^{1}H and ^{13}C NMR spectra for all new compounds and X-ray crystal structure of compound **6a** (PDF)

Cartesian coordinates of all computed structures (TXT)

X-ray crystallographic data for compound **6a** (CIF)

The crystallographic data for compound **6a** have also been deposited with the Cambridge Crystallographic Data Centre (CCDC 1016110).

■ AUTHOR INFORMATION

Corresponding Author

*E-mail: P.Kaye@ru.ac.za.

Notes

The authors declare no competing financial interest.

■ ACKNOWLEDGMENTS

The authors thank Rhodes University for a bursary (to T.O.O.). This work is based upon research supported by the National Research Foundation (NRF; South Africa: IFR2011032500034) and Rhodes University. T.O.O. gratefully acknowledges Obafemi Awolowo University (Ile-Ife, Nigeria) for study leave. M.R.C. thanks the University of Cape Town and the NRF (South Africa: IFR201132500034) for research support. Any opinion, findings, and conclusions or recommendations expressed in this material are those of the authors, and therefore, the NRF does not accept any liability in regard thereto.

■ REFERENCES

(1) (a) Baylis, A. B.; Hillman, M. E. D. German Patent 2155113, 1972. (b) Takizawa, S.; Rémond, E.; Arteaga, F. A.; Yoshida, Y.; Sridharan, V.; Bayardon, J.; Jugé, S.; Sasai, H. *Chem. Commun.* **2013**, *49*, 8392−8394. (c) Peng, C.; Joy, A. *Macromolecules* **2014**, *47*, 1258−1268. (d) Verma, P.; Verma, P.; Sunoj, R. B. *Org. Biomol. Chem.* **2014**, *12*, 2176−2179. (e) Basavaiah, D.; Veeraraghavaiah, G.; Badsara, S. S. *Org. Biomol. Chem.* **2014**, *12*, 1551−1555. (f) Yin, Y.; Sun, G.; Zhang, H.; Zhou, H.; Wu, F. *Chin. J. Chem.* **2014**, *32*, 365−369. (g) Bharadwaj, K. C. *RSC Adv.* **2015**, *5*, 75923. (h) Xie, P.; Huang, Y. *Org. Biomol. Chem.* **2015**, *13*, 8578.

(2) (a) Morita, K.; Suzuki, Z.; Hirose, H. *Bull. Chem. Soc. Jpn.* **1968**, *41*, 2815. (b) Morita, K. Japanese Patent 6803364, 1968.

(3) (a) Basavaiah, D.; Rao, K. V.; Reddy, R. J. *Chem. Soc. Rev.* **2007**, *36*, 1581−1588. (b) Singh, V.; Batra, S. *Tetrahedron* **2008**, *64*, 4511−4574. (c) Basavaiah, D.; Reddy, B. S.; Badsara, S. S. *Chem. Rev.* **2010**, *110*, 5447−5674. (d) Wei, Y.; Shi, M. *Chem. Rev.* **2013**, *113*, 6659−6690. (e) Ciganek, E. *Org. React.* **1997**, *51*, 201−350.

(4) (a) Familoni, O. B.; Kaye, P. T.; Klaas, P. J. *Chem. Commun.* **1998**, 2563−2564. (b) Familoni, O. B.; Klaas, P. J.; Lobb, K. A.; Pakade, V. E.; Kaye, P. T. *Org. Biomol. Chem.* **2006**, *4*, 3960−3965.

(5) Kaye, P. T.; Musa, M. A.; Nocanda, X. W.; Robinson, R. S. *Org. Biomol. Chem.* **2003**, *1*, 1133−1138.

(6) (a) Kaye, P. T.; Nocanda, X. W. *Synthesis* **2001**, 2389−2392. (b) Kaye, P. T.; Nocanda, X. W. *J. Chem. Soc., Perkin. Trans. 1* **2002**, 1318−1323.

(7) Olomola, T. O.; Klein, R.; Lobb, K. A.; Sayed, Y.; Kaye, P. T. *Tetrahedron Lett.* **2010**, *51*, 6325−6328.

(8) Olomola, T. O.; Klein, R.; Mautsa, N.; Sayed, Y.; Kaye, P. T. *Bioorg. Med. Chem.* **2013**, *21*, 1964−1971.

(9) Didierjean, J.; Isel, C.; Querre, F.; Mouscadet, J.-F.; Aubertin, A.-M.; Valnot, J.-Y.; Piettre, S. R.; Marquet, R. *Antimicrob. Agents Chemother.* **2005**, *49*, 4884−4894.

(10) Wang, Z.; Bennett, E. M.; Wilson, D. J.; Salomon, C.; Vince, R. *J. Med. Chem.* **2007**, *50*, 3416−3419.

(11) (a) Dayam, R.; Gundla, R.; Al-Mawsawi, L. Q.; Neamati, N. *Med. Res. Rev.* **2008**, *28*, 118−154. (b) Bodiwala, H. S.; Sabde, S.; Gupta, P.; Mukherjee, R.; Kumar, R.; Garg, P.; Bhutani, K. K.; Mitra, D.; Singh, I. P. *Bioorg. Med. Chem.* **2011**, *19* (3), 1256−1263.

(12) Idahosa, K. C.; Lee, Y.-C.; Nyoni, D.; Kaye, P. T.; Caira, M. R. *Tetrahedron Lett.* **2011**, *52*, 2972−2976.

(13) (a) Hill, J. S.; Isaacs, N. S. *J. Phys. Org. Chem.* **1990**, *3*, 285−290. (b) Bode, M. L.; Kaye, P. T. *Tetrahedron Lett.* **1991**, *32*, 5611−5614. (c) Price, K. E.; Broadwater, S. J.; Jung, H. M.; McQuade, D. T. *Org. Lett.* **2005**, *7*, 147−150. (d) Price, K. E.; Broadwater, S. J.; Walker, D. J.; McQuade, D. T. *J. Org. Chem.* **2005**, *70*, 3980−3987. (e) Robiette, R.; Aggarwal, V. K.; Harvey, J. N. *J. Am. Chem. Soc.* **2007**, *129*, 15513−15525.

(14) Olomola, T. O.; Klein, R.; Kaye, P. T. *Synth. Commun.* **2012**, *42*, 251−257.

(15) Tiekenk, E. R. T. In *Organic Crystal Engineering: Frontiers in Crystal Engineering*; Tiekenk, E. R. T., Vittal, J., Zaworotko, M., Eds.; John Wiley & Sons: Chichester, U.K., 2010; Chapter 6, pp 191−192.

(16) Bernstein, J.; Davis, R. E.; Shimoni, L.; Chang, N. L. *Angew. Chem., Int. Ed. Engl.* **1995**, *34*, 1555−1573.

DOI: 10.1021/acs.joc.5b02372
J. Org. Chem. 2016, 81, 109−120

(17) Frisch, M. J.; Trucks, G. W.; Schlegel, H. B.; Scuseria, G. E.; Robb, M. A.; Cheeseman, J. R.; Montgomery, J. A., Jr.; Vreven, T.; Kudin, K. N.; Burant, J. C.; Millam, J. M.; Iyengar, S. S.; Tomasi, J.; Barone, V.; Mennucci, B.; Cossi, M.; Scalmani, G.; Rega, N.; Petersson, G. A.; Nakatsuji, H.; Hada, M.; Ehara, M.; Toyota, K.; Fukuda, R.; Hasegawa, J.; Ishida, M.; Nakajima, T.; Honda, Y.; Kitao, O.; Nakai, H.; Klene, M.; Li, X.; Knox, J. E.; Hratchian, H. P.; Cross, J. B.; Bakken, V.; Adamo, C.; Jaramillo, J.; Gomperts, R.; Stratmann, R. E.; Yazyev, O.; Austin, A. J.; Cammi, R.; Pomelli, C.; Ochterski, J. W.; Ayala, P. Y.; Morokuma, K.; Voth, G. A.; Salvador, P.; Dannenberg, J. J.; Zakrzewski, V. G.; Dapprich, S.; Daniels, A. D.; Strain, M. C.; Farkas, O.; Malick, D. K.; Rabuck, A. D.; Raghavachari, K.; Foresman, J. B.; Ortiz, J. V.; Cui, Q.; Baboul, A. G.; Clifford, S.; Cioslowski, J.; Stefanov, B. B.; Liu, G.; Liashenko, A.; Piskorz, P.; Komaromi, I.; Martin, R. L.; Fox, D. J.; Keith, T.; Al-Laham, M. A.; Peng, C. Y.; Nanayakkara, A.; Challacombe, M.; Gill, P. M. W.; Johnson, B.; Chen, W.; Wong, M. W.; Gonzalez, C.; Pople, J. A. *Gaussian 03*, revision C.02; Gaussian, Inc.: Wallingford, CT, 2004.
(18) Khene, S.; Lobb, K.; Nyokong, T. *Electrochim. Acta* **2010**, *56* (2), 706−716.
(19) Perkin, W. H. *J. Chem. Soc.* **1868**, *21* (53), 181−186.
(20) Ranu, B. C.; Jana, R. *Eur. J. Org. Chem.* **2006**, *2006*, 3767−3770.
(21) Patre, R. E.; Parameswaran, P. S.; Tilve, S. G. *ARKIVOC* **2011**, *2011* (ix), 68−76.
(22) Jeon, J.-H.; Yang, D.-M.; Jun, J.-G. *Bull. Korean Chem. Soc.* **2011**, *32*, 65−70.
(23) Stoker, J. R.; Bellis, D. M. *J. Biol. Chem.* **1962**, *237* (7), 2303−2305.
(24) Haskins, F. A.; Williams, L. G.; Gorz, H. J. *Plant Physiol.* **1964**, *39*, 777−781.
(25) Bayoumi, S. A. L.; Rowan, M. G.; Blagbrough, I. S.; Beeching, J. R. *Phytochemistry* **2008**, *69*, 2928−2936.
(26) Dennington, R.; Keith, T.; Millam, J. *GaussView*, version 4.1; Semichem Inc.: Shawnee Mission, KS, 2009.
(27) Schaftenaar, G.; Noordik, J. H. *J. Comput.-Aided Mol. Des.* **2000**, *14*, 123−134.

DOI: 10.1021/acs.joc.5b02372
J. Org. Chem. 2016, 81, 109−120